Journal of Chromatography A, 1218 (2011) 2413–2424

Contents lists available at ScienceDirect

Journal of Chromatography A

journal homepage: www.elsevier.com/locate/chroma

Adsorption behavior of large plasmids on the anion-exchange methacrylate monolithic columns

Nika Lendero Krajnc[a,b], Franc Smrekar[a], Aleš Štrancar[a,b], Aleš Podgornik[a,b,*]

[a] BIA Separations d.o.o., Teslova 30, SI-1000 Ljubljana, Slovenia
[b] The Centre of Excellence for Biosensors, Instrumentation and Process Control – COBIK, Velika pot 22, SI-5250 Solkan, Slovenia

ARTICLE INFO

Article history:
Available online 21 December 2010

Keywords:
Plasmids
Monoliths
Convective interaction media (CIM)
Dynamic binding capacity
Purification
Pressure drop

ABSTRACT

The objective of this study was to investigate the behavior of large plasmids on the monolithic columns under binding and nonbinding conditions. The pressure drop measurements under nonbinding conditions demonstrated that the flow velocities under which plasmid passing monolith became hindered by the monolithic pore structure depended on the plasmid size as well as on the average monolith pore size; however, they were all very high exceeding the values encountered when applying CIM monolithic columns at their maximal flow rate. The impact of the ligand density and the salt concentration in loading buffer on binding capacity of the monolith for different sized plasmids was examined. For all plasmids the increase of dynamic binding capacity with the increase of salt concentration in the loading solution was observed reaching maximum of 7.1 mg/mL at 0.4 M NaCl for 21 kbp, 12.0 mg/mL at 0.4 M NaCl for 39.4 kbp and 8.4 mg/mL at 0.5 M NaCl for 62.1 kbp. Analysis of the pressure drop data measured on the monolithic column during plasmid loading revealed different patterns of plasmid binding to the surface, showing "car-parking problem" phenomena under certain conditions. In addition, layer thickness of adsorbed plasmid was estimated and at maximal dynamic binding capacity it matched calculated plasmid radius of gyration. Finally, it was found that the adsorbed plasmid layer acts similarly as the grafted layer responding to changes in solution's ionic strength as well as mobile phase flow rate and that the density of plasmid layer depends on the plasmid size and also loading conditions.

1. Introduction

The use of plasmid DNA (pDNA) as a vector for gene therapy and particularly for DNA vaccination has been extensively investigated during the last decade. Despite poor immunogenicity that it is often stated as a main disadvantage, pDNA vectors have inherent advantages over viral vectors, including safety and production simplicity [1]. Therefore, the percentage of naked/plasmid DNA vectors among all the vectors used in gene therapy clinical trials grew from 11% in year 2002 to 17.7% in 2009 [2]. In 2007 the U.S. Department of Agriculture issued a conditional license for a plasmid DNA vaccine to treat canine melanoma [3,4]. In the same year first phase 3 clinical trial of pDNA based product for human patients with angiogenesis was successfully finished and a new drug application for treatment of critical limb ischemia is now under review by Japanese Ministry of Health, Labor and Welfare [5]. Additionally, investigations of DNA vaccines generated very encouraging results in treatments against malaria and AIDS [6–8] and because of relatively fast production process in comparison to conventional virus-based vaccines, DNA vaccines are also being explored for their utility in influenza vaccination [9,10].

At present, most clinical trials involve plasmids from 5 to 20 kbp in size. However, future requirements for multigene vectors including extensive control regions may require the production of larger plasmids or even mega-sized artificial chromosomes [11]. The target form, most stable for the therapeutic use, is supercoiled (*sc*) pDNA, which is, however, still very sensitive and can be degraded during the purification process [12]. The degree of degradation due to shear forces increases severely with the plasmid size [11,13].

Despite these problems, the rapid evolution of gene therapy and DNA vaccines results in an increasing interest in producing large quantities of pharmaceutical grade pDNA [14–16]. Downstream processing of plasmid DNA usually comprises of several chromatographic steps using different types of interactions [17]. Most of the chromatographic resins used for biotechnological processes are optimized for purification of much smaller proteins, consequently their capacity for bigger molecules such as plasmid DNA is rather low [17,18]. However, chromatographic matrixes suitable for purification of large shear-sensitive particles should not only exhibit high capacity for large molecules but also be highly permeable not to damage the molecules. In addition, their active surface

* Corresponding author at: BIA Separations d.o.o., Teslova 30, SI-1000 Ljubljana, Slovenia. Tel.: +386 1 426 56 49; fax: +386 1 426 56 50.
E-mail address: ales.podgornik@monoliths.com (A. Podgornik).

0021-9673/$ – see front matter © 2010 Elsevier B.V. All rights reserved.
doi:10.1016/j.chroma.2010.12.058

should be available by convective transport in order to avoid slow diffusion of large molecules resulting in long process times that can also lead to degradation of target molecules. Because of that only few chromatographic matrixes are currently effective for purification of large biomolecules, such as superporous supports [19,20], monoliths [21–24] and adsorptive membranes [25]. Convective interaction media (CIM) anion-exchange methacrylate monolithic columns have already been successfully used in the industrial scale purification process of pharmaceutical grade small plasmid DNA [12]. Additionally, developing new hydrophobic interaction CIM methacrylate monoliths enabled the purification of pDNA solely on monolithic columns [24]. Last but not least, it has also been shown recently that monolithic structure is suitable for purification of plasmids with the size up to 62 kbp [23].

The objective of this study was to investigate the chromatographic behavior of large plasmids on the monolithic columns. The impact of chromatographic system and methacrylate monolithic column on the degradation of plasmid molecules was studied and the capacity measurements varying salt concentration in loading buffer were performed for different sized plasmids. By analyzing pressure drop data some physical features of the plasmids in the flow solution as well as of the plasmids being adsorbed on the surface were characterized. Implementing this results some parameters of downstream process could be optimized.

2. Materials and methods

2.1. Materials and instrumentation

All CIM diethylaminoethyl (DEAE) weak anion exchange monolithic columns, 8 mL tube, 76 μL analytical column prototype and custom made 12 μL microanalytical columns packed into CIM 8 mL tube housing or specially designed stainless steel housing for analytical columns, were obtained from BIA Separations (Ljubljana, Slovenia). Plasmids R388, R6K and TP114 (hosts: *Escherichia coli*) were purchased from DSMZ (Braunschweig, Germany) and plasmid pEGFP-N1 (host: *Escherichia coli* DH5α) was purchased from Clontech Laboratories (Mountain View, CA 94043). pDNA conformations and RNA were analyzed by agarose gel electrophoresis (AGE, Bio-Rad, Richmond, VI, USA). Plasmid lengths were determined using 1 kbp Plus DNA Ladder (Invitrogen, Eugene, OR, USA). Agarose gel was made of SeaKem LE Agarose (Lonza Group, Basel, Switzerland) and TBE buffer (40 mM Tris, 20 mM boric acid, 1 mM EDTA, pH 8.0). Luria–Bertani broth, potassium acetate, tris(hydroxymethyl)aminomethane (Tris), boric acid, sodium chloride, sodium hydroxide and hydrochloric acid (37%) were obtained from Merck (Darmstadt, Germany). Antibiotics ampicillin, kanamycin and sulfanilamide, sodium dodecyl sulfate (SDS) and DNase-free ribonuclease A (RNase A) from bovine pancreas were purchased from Sigma (St. Louis, MO, USA). Ethylenediaminetetraacetic acid disodium salt dihydrate (EDTA) was obtained from Kemika (Zagreb, Croatia). All solutions were prepared using water purified by a Watek IWA-80 roi (Ledeč nad Sázavou, Czeck Republic) water purification system and analytical grade reagents. Buffer solutions were prepared by dissolving a known mass of buffering species into ca. 80% of the desired final volume of deionized water, titrating with HCl and adding the deionized water to yield the final solution volume. Finally, buffers were filtered through a 0.45 μm pore size filter composed of Sartolon polyamide (Sartorius, Goettingen, Germany).

Cell density, pDNA purity and concentration were measured by spectrophotometer Smart Spec 3000 (BioRad, Richmond, VI, USA), sample centrifugations and sample analysis were performed using Sorvall RC5C Plus centrifuge (Kendro, Newtown, CT, USA) and agarose gel electrophoresis (AGE, BioRad, Richmond, VI, USA), respectively. All chromatographic experiments were performed using a gradient Knauer HPLC system (Berlin, Germany) consisting of two Knauer Type 64 analytical pumps, an injection valve with 100, 500 or 1000 μL sample loops, a Knauer UV–vis absorbance detector model K-2500 with a 10 mm optical path cell and a conductivity monitor Amersham Biosciences (GE Healthcare, Uppsala, Sweden), all connected via a Knauer interface box to a personal computer for real time data acquisition by Eurochrom 2000 software. For loading the sample into an 8 mL tube the peristaltic pump (Ismatec, Glattbrugg, Switzerland) was used. During pulse response and capacity measurements pressure drop on the monolithic columns was measured by differential manometer (MidWest Instruments, Sterling Heights, MI, USA).

2.2. Methods

2.2.1. Cell lysis protocol

Bacteria were lysed using modified alkaline lysis procedure according to Birnboim and Doly [26]. The liquid cultures of the bacterium *Escherichia coli* with different plasmids were cultivated overnight at 37 °C on Luria–Bertani broth containing proper antibiotic. After harvest, cells were resuspended in TE buffer (50 mM Tris with 10 mM EDTA), pH 8.0, containing 100 μg/mL DNase-free RNase and treated with cell lysis buffer containing 0.2 M NaOH and 1% SDS followed by neutralizing solution (3 M potassium acetate, adjusted to pH 5.5 with glacial acetic acid, chilled to 4 °C). Precipitated material, including cell debris, most chromosomal DNA, some RNA and proteins, was removed by centrifugation at 9000 × *g* for 10 min followed by clarification through a 0.45/0.2 μm Sartobran P filter (Sartorius, Goettingen, Germany).

2.2.2. Purification of plasmids

Plasmid purification was performed by AEX chromatography as described in literature [23]. For this purpose 8 mL CIM DEAE tube monolithic column with ligand density 0.4 mmol/g and average pore diameter 1400 nm was used. Conductivity of the plasmid sample solution, obtained after alkaline lysis, was adjusted to proper value (*i.e.*, the value where RNA does not bind to the column) by adding NaCl. The column was first equilibrated with TE buffer (50 mM Tris with 10 mM EDTA) with NaCl, pH 7.2, with the same conductivity as sample solution. After that plasmid sample was loaded and column was washed with loading buffer. The elution step was performed by linear gradient to TE buffer with 1.5 M NaCl, pH 7.2. Collected plasmid fractions were analyzed for RNA content by anion exchange chromatography (AEC) and AGE. Finally, pure plasmid was precipitated by 2-propanol and dissolved in appropriate buffer.

2.2.3. Electrophoresis and sample purity and quantity

Agarose electrophoresis was run in a horizontal gel electrophoresis. The running buffer was TBE (40 mM Tris, 20 mM boric acid, 1 mM EDTA, pH 8.0). Method was performed for 60 min at 80 V. For staining ethidium bromide was used. Additionally, DNA concentration and purity were measured by spectrophotometer. One unit of OD 260 nm in a 10 mm cuvette corresponded to 50 μg/mL dsDNA. Absorption measurements were taken at wavelengths of 260 nm and 280 nm and 260/280 absorption ratios were calculated from the absorption readings. The absorption ratios of clarified cell lysates were between 1.9 and 2.2 and of pure plasmid samples between 1.8 and 2.0. Protein concentrations were between 100 and 200 μg/mL for clarified cell lysates and under 20 μg/mL for pure plasmid samples, estimated according to Bradford method [27]. The absence of RNA was additionally confirmed by AEC on prototype CIM DEAE analytical monolithic column (column volume (CV) 76 μL) with 0.4 mmol/g ligand density and average pore diameter 1400 nm. The column was first equilibrated with TE buffer, pH 7.2,

then 20 μL of sample was injected onto the column at 1 mL/min (395 cm/h) and gradually eluted by 100 CV linear gradient to TE buffer with 1.5 M NaCl, pH 7.2. Absorbance at 260 nm and conductivity were followed.

2.2.4. Loading under nonbinding and binding conditions (capacity measurements)

Loading under nonbinding conditions was performed on two prototype CIM DEAE analytical monolithic columns (CV 76 μL, 4.4 mm ID × 5 mm *L* bed height) with 2.8 and 2.3 mmol/g ligand density and an average pore diameter of 1400 and 2100 nm, respectively. To avoid any adsorption effects, samples were prepared by dissolving prepurified plasmids in TE buffer with high salt concentration (50 mM Tris, 10 mM EDTA, 1.5 M NaCl, pH 7.2). 100 μL of plasmid sample was injected into the HPLC system at different flow rates (*i.e.*, linear flow velocities). To exclude the effects of chromatographic system the samples were injected into the HPLC system with an empty housing as well as into the system with the monolithic column. The recovery was determined by following absorbance at 260 nm and calculating the ratio between sample peak areas for measurements with the empty housing and the monolithic column. Pressure drop on the empty housing and the monolithic column before and after the sample injection was measured and the difference was calculated to study the impact of flow rate onto the plasmid passing. Collected 1 mL fractions were analyzed by AGE analysis for plasmid isoform degradation.

For capacity measurements custom made CIM DEAE monolithic columns of 12 μL monolith volume (4 mm ID × 1 mm L bed height), average pore diameter 1400 or 2100 nm and various ligand densities were used. Pure plasmid was dissolved in TE binding buffer solution having various pH and NaCl concentrations. The sample was loaded onto equilibrated monolithic column by consecutive injections. Knowing the sample concentration and the sample injected volume the mass of loaded plasmid could be calculated. Measuring absorbance at 260 nm and calculating the ratio between the sample peak area obtained under binding conditions (A) and the sample peak area obtained under nonbinding conditions (A_o, determined separately) the amount of adsorbed plasmid after each injection was estimated and a normalized breakthrough curve (A/A_o) was established. Binding capacities were determined at 50% of the breakthrough curve. Plasmid was then eluted by stepwise change to the TE buffer containing 1.5 M NaCl with the same pH as binding buffer and the elution recovery was calculated as mass of eluted plasmid divided by mass of adsorbed plasmid.

2.2.5. Atomic force microscopy

Purified plasmid samples of 39.4 kbp plasmid were examined with an atomic force microscope (AFM, Solver PRO, NT-MDT, Russia) in the tapping mode in air at room temperature. The samples were scanned with standard Si cantilever with a force constant of 10 N/m and at a resonance frequency of 170 kHz. Plasmid DNA samples for AFM imaging were prepared by placing a drop of pDNA solution onto the freshly cleaved mica surface. After 3 min incubation at room temperature, it was rinsed with 0.1 M $MgCl_2$, deionized water, and air dried afterwards.

2.3. Calculations

2.3.1. Pressure drop measurements and plasmid layer thickness

The pressure drop on the monolithic columns was measured using differential manometer. The data was analyzed by Darcy's law [28]:

$$\frac{\Delta P}{L} = \frac{\eta}{B_o} \cdot u \tag{1}$$

where ΔP is the pressure drop on the monolith (Pa), L the column length (bed height, m), η the mobile phase viscosity (Pa s), B_o the column permeability (m^2) and u is the superficial velocity (m/s) calculated as $u = \phi_v/S$ (ϕ_V is the volume flow rate (m^3/s) and S is the cross sectional area of the chromatographic support (m^2)). Pressure drop on the monolith was calculated as a difference between pressure drop on the monolithic column and the empty housing. To compare the pressure drop under different conditions (flow rate and buffer composition) the inversed permeability was calculated as:

$$\frac{1}{B_o} = \frac{\Delta P}{\eta L u} \tag{2}$$

To estimate the thickness of the adsorbed plasmid layer from pressure drop measurements the equation developed for calculating pore diameter of grafted monolith was used [29]:

$$d_a = d\sqrt{\frac{\sqrt{\varepsilon^2(B_a/B) + 4\sqrt{B_a/B}(1-\varepsilon)} - \varepsilon\sqrt{B_a/B}}{2(1-\varepsilon)}} \tag{3}$$

where d is the pore diameter (nm) and ε the column porosity. Subscript a stands for monolith with adsorbed plasmid. The layer thickness of adsorbed plasmid, h (nm), was calculated using following equation:

$$h = \frac{d - d_a}{2} \tag{4}$$

2.3.2. Radius of gyration

The radius of gyration for supercoiled plasmid was calculated from equations [30]:

$$R_G = 0.715\,(R_{G\text{-}OC}) = 0.715\sqrt{\left(\frac{1}{2}R^2_{G\text{-}Linear}\right)} \tag{5}$$

where $R_{G\text{-}OC}$ and $R_{G\text{-}Linear}$ are the radii of gyration of the open-circular and the linear plasmid isoforms, respectively. The radius of gyration of the plasmid linear form was calculated using "worm-like chain" model [31]:

$$R_{G\text{-}Linear} = a\left[\frac{L}{3a} - 1 + \frac{2a}{L} - 2\left(\frac{a}{L}\right)^2\left(1 - e^{-L/a}\right)\right]^{1/2} \tag{6}$$

where L is the contour length (the number of DNA base pairs (bp) multiplied by the axial rise per bp, 0.34 nm/bp) and a the persistence length (the measure of chain stiffness) in nm. The persistence length is a function of the solution ionic strength and can be calculated from following equation [32]:

$$a = \left(\frac{\pi a^*}{2}\right)^{2/3}\frac{R^{4/3}}{Z^2\ell_B}\left[(2Z\xi - 1)\frac{\kappa b e^{-\kappa b}}{1 - e^{-\kappa b}} - 1 - \ln\left(1 - e^{-\kappa b}\right)\right] \tag{7}$$

where $a^* = 7.4$ nm is the persistence length of a hypothetically uncharged DNA, $R = 1$ nm is the radius of the DNA double-helix. Z is the valence of the salt cation ($Z = +1$ for Na^+), $\ell_B = 0.71$ nm at room temperature is the Bjerrum length for pure water, κ is the inverse Debye length, ξ is the DNA charge density ($= \ell_B/b$) and b is the spacing between DNA charge sites (0.17 nm). κ was estimated by equation $\kappa^{-1} = 1/\sqrt{8\pi\ell_B N_A I}$, where N_A is the Avogadro number and I is the ionic strength of the solution having molarity units.

3. Results and discussion

Production of plasmid DNA involves fermentation, cell lysis and purification steps. Purification process of large biomolecules usually comprises of several chromatographic steps using different types of interactions. These processes are already well developed and optimized for plasmids of size up to 10 kbp [24,33], but their

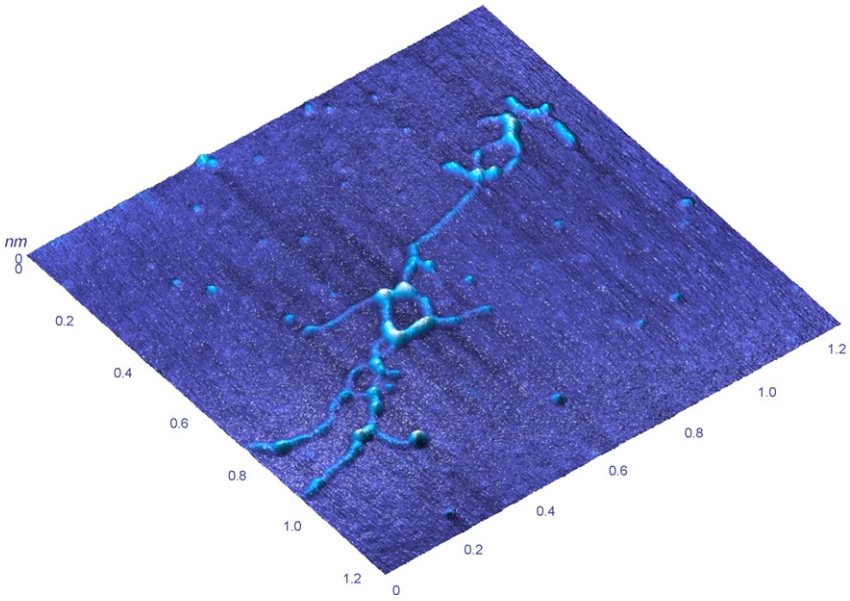

Fig. 1. AFM picture of 39.4 kbp large plasmid.

application might not be straightforward for larger plasmids since the stability of the plasmid exposed to the shear forces decreases drastically with its size [11,13,34]. However, it has been shown recently that using CIM methacrylate monolith, the purification of plasmids with the size up to 62 kbp is possible without significant degradation of *sc* form [23]. This is quite surprising taking into account plasmid dimensions and monolith pore size ratio as well as high strength of the interaction between these highly charged molecules and a stationary phase [35,36]. Therefore, further studies have been performed to understand plasmid behavior under binding and non-binding conditions.

3.1. Non-binding conditions

To explore the behavior of plasmids passing the monolithic column under non-binding conditions pDNA samples were injected onto two DEAE monolithic columns with an average pore diameter of 1400 and 2100 nm at different flow rates. To avoid any plasmid adsorption samples contained high salt concentration buffer. The retention volume of the chromatographic peaks coincided with the dead volume of the system confirming that no binding occurred.

Recovery and *sc* form degradation results are summarized in Table 1. Using the monolithic column with the pore size of 1400 nm the *sc* forms of 21, 39.4, and 62.1 kbp plasmids remained intact within the linear velocity range between 80 and 570 cm/h. For the monolithic column with larger pores (2100 nm) the *sc* forms of 21 and 39.4 kbp pDNA did not degrade up to the linear velocity of 990 cm/h, while for 62.1 kbp pDNA limiting velocity was 790 cm/h. Using higher linear velocities plasmids were already damaged by pumping the sample through the HPLC system with an empty housing (data not shown) being consistent with the data in literature [37].

Interestingly, the recoveries for all three tested plasmids were rather independent on the tested monolith pore size. For 21 kbp plasmid the recovery was very high in the whole range of tested linear velocities (around 100% till 400 cm/h while it decreased to around 90% at higher linear velocities up to 990 cm/h). Similarly, recovery for 39.4 kbp plasmid was also high and quite independent on the linear velocity, *i.e.*, for the monoliths with the pore size of

Table 1
Recoveries (%) and *sc* form degradation (*sc*) of large plasmids passing the monolithic column under nonbinding conditions.

Superficial velocity, cm/h	Monolith pore size 1400 nm[a] pDNA size, kbp						Monolith pore size 2100 nm[a] pDNA size, kbp					
	21.0		39.4		62.1		21.0		39.4		62.1	
	%	*sc*	%	*sc*	%	*sc*	%	*sc*	%	*sc*	%	*sc*
82	99[b]	nd[c]	85	nd	85	nd	96	nd	89	nd	91	nd
165	100		87		93		/		99		95	
250	99		88		90		100		92		94	
325	100		89		81		/		98		93	
400	95		86		91		97		96		90	
470	90		94		88		/		100		86	
570	89		96		82		89		98		87	
790							86		97		84	
990							90		91		75	d[d]
1180									/		72	d
1580									94	d		

[a] Monolith volume (CV) 76 μL.
[b] Standard deviation of recovery results is ±5%.
[c] No degradation of *sc* form occurred.
[d] Degradation of *sc* form occurred.

1400 nm the recovery was between 85 and 100% in velocity range of up to 600 cm/h and slightly higher (between 90 and 100%) for the monolith with larger pores at velocities up to 1580 cm/h. On the other hand, recovery for 62.1 kbp plasmid was around 85–100% for velocity up to 470 cm/h and started to decrease at higher flow rates. The decrease of the recovery with the increase of the flow rate was a bit more pronounced for the monolith with smaller pores. The lowest recovery for 62.1 kbp large plasmid was 72% at 1180 cm/h for the monolith with larger pores (for the monolith with smaller pores the highest tested velocity was 600 cm/h where the recovery was 82%).

The decrease in relative peak area (recovery) with increasing flow rate on the monolithic and the perfusive stationary phases was observed for spherical virus particles (adenovirus [38]) and was explained by particle entrapment into pore constrictions. At low flow rates virus can swim out the narrow pore by diffusion, however, at higher flow rates virus will remain trapped [38]. Since diffusion coefficients for plasmids larger than 10 kbp are 2.3×10^{-12} m^2/s and lower [39], what is smaller as for adenovirus particles (3.67×10^{-12} m^2/s [38]), the hydrodynamic diameter that is inversely proportional to diffusion coefficient according to Stokes–Einstein equation [30] is larger for large plasmid as for adenovirus particle. Therefore, for such large molecules that have a shape closer to the branched rope as to the spherical particle (see Fig. 1) the entrapment might be even more pronounced. However, as reported for virus particles [38] also the tested plasmids could be washed out of the monolith by reversed flow. Though, reversing the flow in the case of plasmids was not as efficient as it was shown to be for globular particles (some plasmid molecules still remained entrapped in the monolith; data not shown).

According to the results, it seems that for plasmids with the size up to 40 kbp neither pore size nor flow rate significantly affected the recovery in the tested range, while for larger plasmids the recovery decreased with increasing flow rate and was slightly more pronounced for the monoliths with smaller pore size. Similar experiments were performed by Kong et al. [11]. They measured pDNA transmission through filtration membrane with the pore size of 0.22 μm for plasmids with the size from 6 to 116 kbp. In the range of linear velocities from 6 to 138 cm/h the recovery was independent on the flow rate but linearly decreasing with plasmid size. Since the pore size of used membranes was much smaller than the pore size of tested monolithic columns, the results cannot be directly compared; however, effect of pore size on transmission of various plasmid sizes can be recognized.

To establish whether the transmission of plasmid through the monolithic column changes the column permeability, pressure drop difference on the empty housing and the monolithic column before and after the plasmid injection was followed. Since all the experiments were performed under non-binding conditions using the same mobile phase and monolithic columns of the same dimensions, instead of calculating permeability simply the pressure drop difference at various flow rates was examined. Injecting plasmid sample into the empty column housing resulted in no change in pressure drop before and after plasmid passing even at the highest tested linear velocity (1580 cm/h). Therefore, the pressure drop on the empty housing was not taken into account when analyzing the pressure drop on the monolithic column.

Fig. 2 shows the dependence of the pressure drop difference on the monolithic column before and after the sample injection on the linear flow velocity for various plasmids. Using the monolith with the pore size of 1400 nm the pressure drop on the column did not change after the injection of 21.0 kbp plasmid sample in the range of linear flow velocities up to 600 cm/h. On the other hand, for 39.4 kbp and 62.1 kbp plasmid it started to increase at velocities above 400 and 325 cm/h, respectively. The pressure drop on the monolithic column with 2100 nm pores started to increase after the

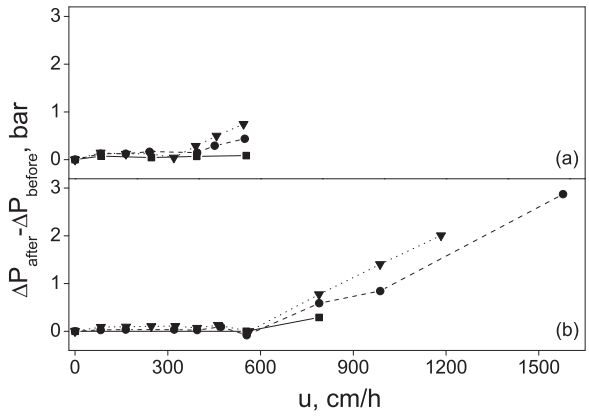

Fig. 2. Impact of superficial linear velocity on pressure drop difference before and after plasmid passing through the monolithic column. Plasmids used: (—■—) 21, (- -●- -) 39.4 and (· · ▼ · ·) 62.1 kbp. pDNA samples were injected onto with CIM DEAE monolithic column (CV 76 μL) with average pore size diameter (a) 1400 and (b) 2100 nm under nonbinding conditions (50 mM Tris + 10 mM EDTA + 1.5 M NaCl buffer, pH 7.2).

plasmid transmission at linear flow velocities above the 570 cm/h. The increase was more pronounced when using samples with larger plasmids. Increase of pressure drop difference with an increase of flow rate was expected, since partial clogging of the pores with large DNA molecules at higher flow rates is possible and had already been observed [37]. These results are also in agreement with the recovery data demonstrating that unhindered passing of large hairy-like molecules depends on the size of the molecule, linear flow velocity and the pore size of the chromatographic support. However, the flow velocities where the transmission of tested plasmids becomes hindered by monolithic pore structure are all very high and exceed the values encountered when running any CIM monolithic column at its maximal flow rate [40].

3.2. Binding conditions

To study plasmid behavior on the monolithic surface under binding conditions the capacity measurements with different sized plasmids were performed. The impact of the mobile phase composition, anion exchange ligand density, plasmid size, pore diameter and flow rate on binding capacity, recovery and column pressure drop was examined.

Varying mobile phase pH from 7 to 9 did not affect the dynamic binding capacity for plasmids larger than 20 kbp. However, at pH 9 the recoveries were higher for about 20% what can probably be attributed to the weaker binding due to a lower degree of ionization of weak anion exchange (DEAE) groups on the monolith. On the other hand, the dynamic binding capacity for large plasmids was drastically dependent on NaCl concentration in the binding buffer solution. As it has already been shown for 39.4 kbp plasmid the capacity at 0.4 M NaCl was almost 6-fold higher as the capacity measured in the absence of salt [23]. These results were quite surprising and further examination of this phenomenon was carried out. Firstly, the same measurements were repeated on DEAE monoliths of the various ligand densities. Fig. 3 shows the dynamic binding capacity of 39.4 kbp large plasmid measured on DEAE monolithic columns with different ligand densities. It can be observed that the capacity is independent on the ligand density at low salt concentrations up to 0.15 M while it becomes highly dependent on the ligand density at higher salt concentrations. This denotes that at very high salt concentrations, when charge screening is very pronounced, high density of anion exchange groups on matrix surface forming strong positive electrostatic field above the surface is necessary to retain large negatively charged plasmids.

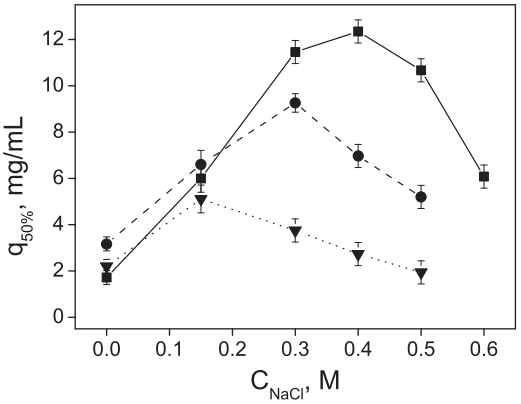

Fig. 3. Dynamic binding capacities for 39.4 kbp plasmid at different NaCl concentrations in binding buffer on DEAE monolithic columns with various ligand densities. Binding buffer used: 50 mM Tris + 10 mM EDTA + x M NaCl buffer, pH 7.2. Monolithic columns (CV 12 μL) used: (—■—) high (2.8 mmol/g), (- -●- -) medium (0.83 mmol/g) and (· · ▼ · ·) low (0.52 mmol/g) ligand density.

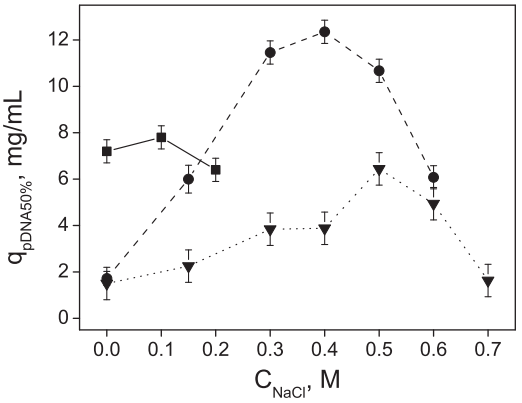

Fig. 4. Dynamic binding capacities for (—■—) 4.7, (- -●- -) 39.4 and (· · ▼ · ·) 62.1 kbp plasmid on DEAE monolithic column. Capacities for 4.7 kbp plasmid were obtained from the literature [29] and were measured on DEAE monolith (CV 0.34 mL) with average pore diameter 1300 nm and 2.2 mmol/g ligand density. Capacities for 39.4 kbp plasmid were measured on high ligand density (2.8 mmol/g) monolith (CV 12 μL) with average pore diameter 1400 nm. Capacities for 62.1 kbp plasmid were measured on high ligand density (2.3 mmol/g) monolith (CV 12 μL) with average pore diameter 2100 nm.

Unlike recovery, which depends mainly on the interaction strength of bound molecule with the charged surface and it is thus higher using low ligand density monolith and high salt concentration in binding buffer (Table 2), the capacity increase cannot be explained only by surface–molecule interactions but also the intermolecular interactions (*i.e.*, interactions between adsorbed macromolecules) has to be taken into account [41].

Furthermore, the capacity measurements with different sized plasmids at various salt concentrations were performed. It can be seen from Fig. 4 that the optimum salt concentration is higher when the plasmid is larger. Though, the highest capacities (expressed in mg/mL) were obtained using 39.4 kbp large plasmid. The recoveries depended on the plasmid size and were smaller when the plasmid was larger (see Table 3).

Capacity measurements with 62.1 kbp large plasmid were performed on two monoliths with various average pore diameters (1400 and 2100 nm) consequently exhibiting different surface area [42]. Data are summarized in Table 4. As it can be seen, the ratio of specific surface areas and the ratio of binding capacities are practically the same, which means that also for such large molecules the accessibility of the monolithic surface is the same and the capacity difference is a consequence solely of specific surface area difference. However, recovery was considerably lower using monolith with smaller pores probably due to the molecule entrapment (see also Section 3.1). Consequently, amount of eluted plasmid was practically the same for both monoliths, so the use of the monolith with larger pores seems to be more economic since sample loss is smaller. Moreover, the pressure drop on the monolith with smaller pores increased much faster with the amount of the adsorbed plasmid. For example, during loading of 75 μg of 62.1 kbp plasmid (that is equal to the capacity of 6.3 mg/mL) at linear flow velocity of 100 cm/h the pressure drop on the monolith with 1400 nm pore size raised from 0.6 to 13.9 bar, while on the monolith with 2100 nm pores the pressure drop increase was only from 0.1 to 3.8 bar which is almost 4 times lower as for the monolith with smaller pores.

High salt concentration has several effects on charged plasmid molecules and the extreme capacity increase is probably the consequence of their combination. Firstly, the geometry of plasmid molecules depends dramatically on ionic conditions of the solution [43]. It was reported that increasing NaCl concentration from 10 to 100 mM the superhelix diameter decreases for nearly 50% [44] and adopts highly compact and bent interwound shape; therefore, at higher salt concentration one plasmid molecule would cover smaller surface area. However, further increase in salt concentration (*i.e.*>0.1 M NaCl) did not affect the superhelix diameter anymore. Assuming that plasmid dimensions shrink for 50% in all directions, its surface coverage lowers to ¼ of initial value and the capacity would therefore show maximally 4-fold increase. Calculating the radius of gyration for 39.4 kbp plasmid at various salt concentrations (Eqs. (5–7)) the actual decrease of the radius in the region of salt concentrations between 0 and 0.6 M was only 20%, which would consequently increase the capacity for only approximately 50%. This shows that shrinking of the plasmid could not be the only cause for 6-fold increase in binding capacity. Addition of the salt to binding buffer also screens strong negative electrostatic charge of plasmid molecules and decreases repulsion between adjacent phosphate groups on the molecule backbone, so the persistence length that is a measure of the DNA structural rigidity decreases and the molecule can better fit surface topology [32]. Moreover, charge screening also decreases repulsion between plasmid molecules, thus they can be packed more closely on the monolithic surface [41]. Another explanation for capacity increase

Table 2
Average recoveries of eluted 39.4 kbp large plasmid using binding buffer without salt and with addition of salt for DEAE monoliths with different ligand densities.[a]

DEAE monolith	Binding buffer without NaCl	Binding buffer with concentration of NaCl from 0.15 to 0.5 M[b]	Binding buffer with 0.6 M NaCl
LLD[c]	88[d]	86	/
MLD[e]	57	78	/
HLD[f]	40	71	90

[a] Monolith volume (CV) 12 μL. Monolith pore size 1400 nm.
[b] As the recoveries of eluted plasmid loaded in binding buffer with salt were very similar for all salt concentrations used, the average recovery is given.
[c] Low ligand density monolith (see also text below Fig. 3).
[d] Recovery data are given in %. Standard deviation is ±5%.
[e] Medium ligand density monolith (see also text below Fig. 3).
[f] High ligand density monolith (see also text below Fig. 3).

Table 3
Average recoveries for different sized plasmids using binding buffer without and with addition of salt for DEAE monoliths with high ligand density.[a]

Plasmid size, kbp	Binding buffer without NaCl	Binding buffer with NaCl (average for different salt concentrations)
4.7	80[b]	100[c]
39.4	40	73[d]
62.1	28	64[e]

[a] For conditions see Fig. 4.
[b] Recovery data are given in %. Standard deviation is ±5%.
[c] Average for 0.1 and 0.2 M NaCl in binding buffer.
[d] Average for NaCl concentration in binding buffer from 0.15 to 0.6 M.
[e] Average for NaCl concentration in binding buffer from 0.15 to 0.7 M.

Table 4
Comparison of specific surface area, binding capacity and recovery for 62.1 kbp large plasmid for monoliths with different average pore size.[a]

Average pore diameter, nm	Ligand density, mmol/g	Specific surface area[b], m^2/g	Specific surface area ratio	Dynamic binding capacity[c], mg/mL	Dynamic binding capacity ratio	Recovery, %	Mass of eluted plasmid from 1 mL of monolith, mg
1400	2.8	7.9	1.27	8.4 ± 0.5[d]	1.31	51 ± 5	4.3
2100	2.3	6.2		6.4 ± 0.5[e]		66 ± 5	4.2

[a] Monolith volume (CV) 12 μL.
[b] Data obtained from the literature [42].
[c] Dynamic binding capacity was measured at 0.5 M NaCl in binding buffer and linear flow velocity 95 cm/h.
[d] Measurement was performed at 95 cm/h.
[e] Measurement was performed at 190 cm/h.

rises from access to the surface in smaller pores. Plasmid transmission through ultrafiltration membranes was studied by several groups and all of them found that transmission of plasmids was significantly higher in the presence of salt, which means that after the salt addition plasmids could enter the pores that could not be accessed in the absence of salt [11,45,46]. It was also suggested, that capacity increase at higher salt concentrations can be further increased by molecule binding perpendicular to the surface [21], which was recently demonstrated to be entropically driven process [47]. Though this could be a possible mechanism in the case of small plasmids, it seems highly unlikely to work for large plasmids. Since the length of the molecule is the same or even larger as the pore diameter of the monolith (from Fig. 1 it can be seen that the dimensions of 39.4 kbp plasmid are 1.4 μm in one direction, which is the same as the average pore size diameter of the monolith) such binding would be possible only if the molecule would bind across the pore what would close the pore for other plasmids therefore cause clogging.

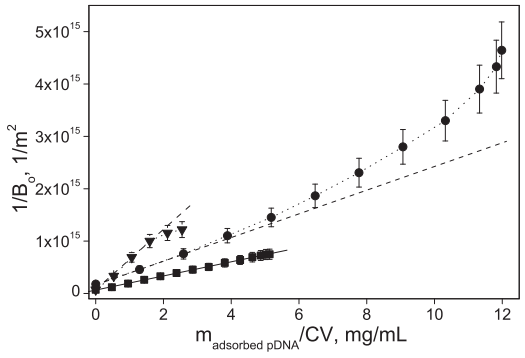

Fig. 5. Examples of inversed permeability change with mass of adsorbed 39.4 kbp plasmid per mL of monolith. (—■—) Linear increase, (··●··) positive and (··▼··) negative deviation from linear increase. Measurements were performed on monolithic columns (CV 12 μL) with average pore size of 1400 nm and (··▼··) 0.83 mmol/g group density using TE binding buffer without salt (B_o of monolith before pDNA loading was 1.4E-14 m^2), (··●··) 2.8 mmol/g group density using TE binding buffer with 0.4 M NaCl (B_o of monolith before pDNA loading was 5.6E-15 m^2), and (—■—) 0.83 mmol/g group density using TE binding buffer with 0.5 M NaCl (B_o of monolith before pDNA loading was 1.4E-14 m^2).

To elucidate possible scenarios, pressure drop on the monolithic column was followed during the capacity measurements and the permeability (B_o) was calculated using Darcy's law (Eq. (1)). Considering pressure drop dependence on the flow rate and viscosity of the solution as follows from Darcy's law, the comparisons were made by inversed permeability ($1/B_o$, Eq. (2)). Interestingly, there were three different profiles of pressure drop (inversed permeability) increase when plotted against a mass of adsorbed 39.4 kbp large plasmid: constant increase (linear), positive and negative deviation from linear increase (see Fig. 5).

Linear increase was typically observed at loading of small plasmids (<10 kbp) on the monolithic column and can be explained by gradual filling of the pores with plasmid DNA [22]. The free cross sectional area available for the liquid flow is evenly reduced, resulting in a constantly increasing pressure drop and hence reducing permeability. Linear increase was observed also for monoliths with medium or small ligand density and NaCl concentration of 0.3 M or higher. If the slope of pressure drop plotted against mass of adsorbed plasmid becomes steeper (positive deviation) this indicates either mechanical entrapment of the molecules or bed collapse, which might result in a complete blocking of the column [37]. Since after plasmid elution and monolith regeneration the results of binding capacities were reproducible, the bed col-

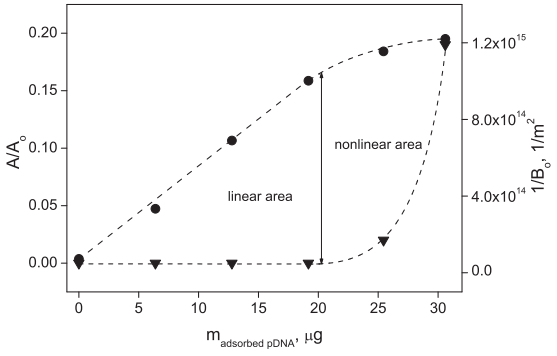

Fig. 6. Normalized breakthrough curve (▼, A/A_o) and inversed permeability change (●) with mass of adsorbed plasmid. Normalized breakthrough curve was obtained by estimating the ratio of the amount of adsorbed and injected plasmid (for detailed description see Section 2.2.4).

Table 5
Rate of inversed permeability change dependent on mass of adsorbed 39.4 kbp large plasmid.

DEAE monolithic column[a]	Concentration of NaCl in binding buffer, M					
	0	0.15	0.3	0.4	0.5	0.6
HLD[b]	5.2E+13[c]	4.9E+13	2.6E+13	2.2E+13	1.8E+13	1.1E+13
MLD[d]	4.9E+13	2.9E+13	2.4E+13	2.0E+13	1.1E+13	/
LLD[e]	5.2E+13	2.7E+13	1.7E+13	9.9E+12	8.4E+12	/

[a] Monolith volume (CV) 12 μL. Monolith pore size 1400 nm.
[b] Monolith with high (2.8 mmol/g) amount of DEAE groups.
[c] In m-2 μg-1 units. Maximum relative standard deviation of slope coefficients was 15%.
[d] Monolith with medium (0.83 mmol/g) amount of DEAE groups.
[e] Monolith low (0.52 mmol/g) amount of DEAE groups.

lapse obviously did not occur. Partial pore clogging with 39.4 kbp plasmid was generally detected using high ligand density monolith and NaCl concentration over 0.3 M when mass of adsorbed plasmid exceeded 8 mg of plasmid per mL of monolith. The last and probably the most interesting pressure drop profile was negative deviation from linearity. This was observed for capacity measurements of 39.4 kbp plasmid in 0.15 M NaCl solutions or in the absence of salt independently on the monolith used. After certain amount of bound plasmid the pressure drop became constant although additional plasmid was adsorbed. Interestingly, the slope of pressure drop curve started to decrease exactly when the breakthrough of plasmid occurred (Fig. 6). Thus the monolith surface was already covered by plasmid molecules and the plasmid layer was impermeable to flow. However, additional molecules were still "parked" (adsorbed) between others on the free monolith surface. Therefore, extra plasmid molecules did not cause further reduction of pore size and so did not influence permeability or pressure drop. This phenomena is described in literature as "steric hindrance model" or "car-parking problem" [48] and explains slower dynamics of the macromolecule adsorption when approaching saturation of chromatographic matrix surface. Unfortunately, no data about the pressure drop were reported for comparison.

On the contrary to 39.4 kbp large plasmid, where such type of the pressure drop behavior was observed only at specific loading conditions, it was typical for 21 kbp plasmid on 1400 nm pore monolith and for 62.1 kbp plasmid on 2100 nm pore monolith. Surprisingly, pressure drop increased linearly for 62.1 kbp plasmid on the monolith with smaller pore size (in TE buffer with 0.5 M NaCl, pH 7.2). Interestingly, the amount of adsorbed 62.1 kbp plasmid in this case was below 8 mg/mL (*i.e.*, 95 μg per 12 μL monolith) which coincides with the data for 39.4 kbp plasmid.

Regardless the type of pressure drop profile its initial part measured at the beginning of sample loading was always linear. In Table 5 the rate of the inversed permeability change by increasing mass of adsorbed plasmid (slope coefficients) for three different monoliths at various salt concentrations are listed. As one can see, the slope depends on the density of AEX groups on the monolith as well as on the salt concentration in loading buffer. Pressure drop increased faster with the mass of adsorbed plasmid if the NaCl concentration in the mobile phase was lower what can be explained by stronger electrostatic repulsion between adjacent molecules and adjacent phosphate groups on the same molecule and consequently larger plasmid dimensions. Because of that, plasmid molecules occupy more space in the pore and cause bigger pressure drop increase on a mass of adsorbed molecules. Addition of salt shields electrostatic interactions and "shrinks" plasmid molecules, so the reduction of pore space at adsorption of one plasmid molecule is smaller and permeability is higher. However, the dependency of pressure drop increase on ligand density is a bit more complicated to explain. It seems that using loading buffer without salt, pressure drop increase (as well as dynamic binding capacity) was independent on ligand density of the monolithic column. On the other hand, using mobile phase solutions with NaCl, slopes were higher for the monoliths with higher ligand densities but also the capacities for plasmid were higher.

To understand the impact of ligand density and salt concentration on the plasmid binding further analysis of pressure drop data were performed. Using Eqs. (3) and (4) the adsorbed plasmid layer thickness was calculated. Furthermore, the monolith surface area was estimated from specific surface area obtained by BET analysis (literature data [42], see also Table 4) and the surface density as well as spatial density of plasmid layer were calculated as mass of the adsorbed plasmid divided by surface area or volume of the adsorbed layer (volume was calculated as a monolith surface area multiplied by a layer thickness), respectively. Layer thickness (Fig. 7a) is a measure that tells us how deep from the pore surface plasmid layer extends and is a consequence of mutual contribution of attraction forces between negatively charged plasmid and positively charged surface and electrostatic repulsion between adjacent phosphate groups on the plasmid molecule. Surface density (Fig. 7b) incorporates proximity of adsorbed plasmid molecules, *i.e.*, packing density of adsorbed molecules, which depends mostly on electrostatic repulsion between adjacent plasmid molecules, and surface area covered by a single plasmid molecule. Last measure that incorporates all described effects is layer density (Fig. 7c).

As we can see from Fig. 7, in the absence of salt all three parameters had the lowest values. Small layer thickness for all three monoliths with various ionic capacities was most probably the consequence of strong attractive electrostatic forces between plasmid molecules and the surface, which also coincided with low recoveries at zero salt concentration (see Tables 2 and 3). The interaction was stronger for the monolith with high AEX group density where layer thickness was the smallest (around 85 nm) and the recovery was the lowest. Low surface and spatial layer density indicated that strong repulsion interactions could force plasmids to adsorb on the surface far away from each other. After addition of salt all three parameters increased. That can be interpreted by two separate effects that are a consequence of charge screening. Firstly, plasmid molecules can adopt highly compact and bent interwound shape [44] and, therefore, can be packed more closely (higher surface and spatial density). The highest packing density on a monolith depended on the AEX group density and became nearly constant after the optimal salt concentration (*i.e.*, the salt concentration at the highest binding capacity). Secondly, addition of salt weakened the interaction between plasmid and monolith surface, which was also shown by higher elution recoveries, so plasmids were not so tightly bound to the surface and they could extent deeply into the pore (bigger layer thickness). Large plasmids do not have a shape of a simple rod, as is quite common for small plasmids (<3 kbp), but they are highly branched molecules with a dynamic shape (Fig. 1). However, if every part of the molecule would be adsorbed on the surface, *i.e.*, if the whole molecule would be lying on the surface, the adsorbed layer thickness would approximately equal to superhelix diameter that is not a function of plasmid size [30,44] and the pres-

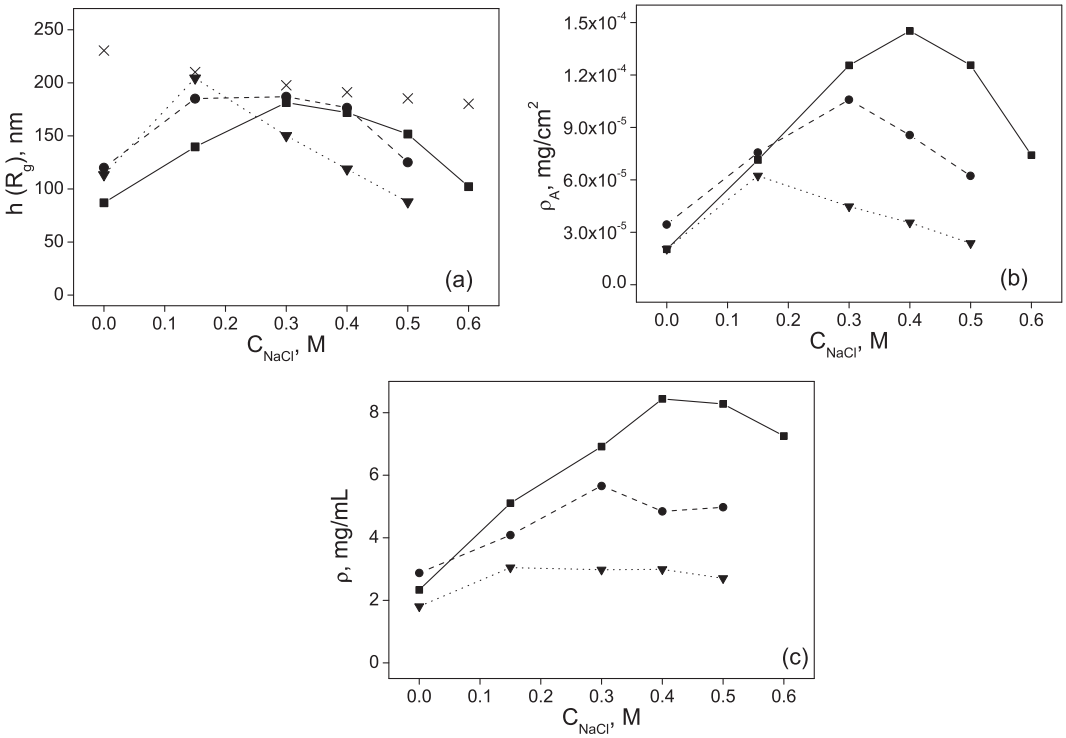

Fig. 7. (a) Plasmid layer thickness in comparison with (×) calculated radius of gyration, (b) layer surface density and (c) spatial layer density for adsorbed 39.4 kbp large plasmid on (—■—) high, (- -●- -) medium and (· · ▼ · ·) low DEAE ligand density monoliths at various NaCl concentrations in binding buffer. RSD is estimated in Table 7.

sure drop would increase equally during loading of plasmids having various size. Since this was not the case and the pressure drop increased faster when larger plasmid was loaded onto the column (Table 7), it seems that several plasmid branches do extend into the pore and that could be detected by pressure drop measurements (for illustration see Fig. 8a).

Comparison of layer thickness for 39.4 kbp plasmid on DEAE monoliths with different ligand densities and radius of gyration for the same plasmid in the solution is given in Fig. 7a. Radius of gyration at different ionic strengths of buffer solution was calculated using Eqs. (5)–(7). As it can be seen from Fig. 7a, the radius of gyration monotonically decreases with the increase of salt concentration in buffer solution, which is a consequence of weaker repulsive interactions between the adjacent phosphate groups and the segments on the same molecule at higher ionic strength and, therefore, smaller size of the molecule [32]. Molecule's radius of gyration depends solely on molecule structure and geometry and solution conditions, while layer thickness reflects a combination of static as well as of dynamic interactions that besides the molecule and the solution characteristics includes also the surface structure and the mobile phase flow rate. From Fig. 7a it can be observed that at salt concentrations, where the binding capacity for the plasmid was maximal and the layer density of the plasmid on monolithic surface was the highest, the layer thickness was very similar to the radius of gyration. Moving towards lower or higher salt concentrations the layer thickness became lower. The difference at lower salt concentrations was most probably a consequence of strong plasmid–surface interactions, described before. However,

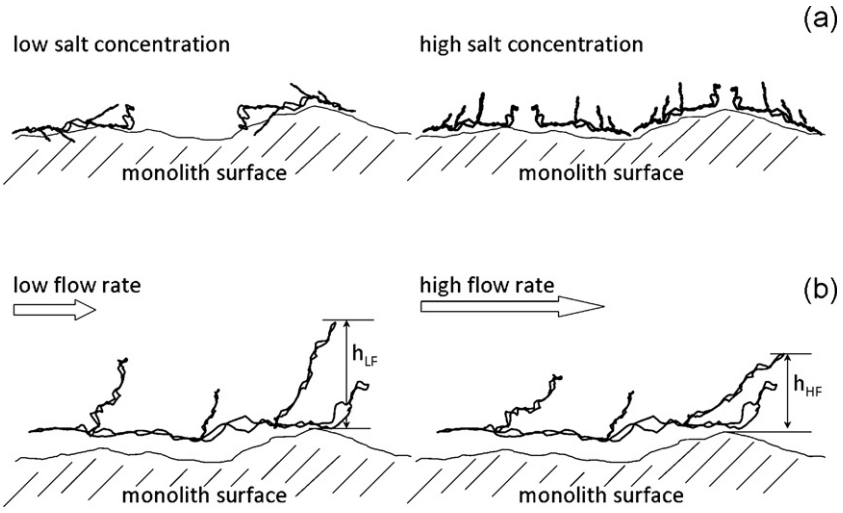

Fig. 8. Schematic illustration of large plasmid adsorption on the monolithic surface at various (a) salt concentrations and (b) flow rates.

Table 6
Binding capacities, recoveries, slope coefficients of inversed permeability dependent on mass of loaded plasmid and adsorbed plasmid thicknesses for 39.4 kbp plasmid at different flow rates.[a]

Linear flow velocity[b], cm/h	$q_{50\%}$[c], mg/mL	Recovery, %	$1/(B_o \cdot m_{R6K})$, $1/(m^2\ \mu g)$	h, nm
120	13.5 ± 0.5	81 ± 5	(3.1 ± 0.4)E +13	210
240	12.4 ± 0.5	84 ± 5	(2.2 ± 0.3)E +13	172
335	12.8 ± 0.5	82 ± 5	(2.1 ± 0.3)E +13	177

[a] Column used: CIM DEAE monolithic column (CV 12 μL) with 1400 nm pore size and 2.8 mmol/g ligand density. Conditions. Loading buffer: 50 mM Tris + 10 mM EDTA + 0.4 M NaCl, pH 7.2. Elution buffer: 50 mM Tris + 10 mM EDTA + 1.5 M NaCl, pH 7.2. Elution was carried out at 190 cm/h for all experiments. Detection: absorbance at 260 nm.
[b] Linear flow velocity was calculated as volumetric flow rate divided by column bed cross-sectional area.
[c] Capacities were determined at 50% of breakthrough.

the resemblance of radius of gyration and layer thickness at higher salt concentrations brought us to the conclusion that the addition of salt could cause that impact of surface attraction on the layer thickness became insignificant and the height of plasmid above the surface was determined mostly by solution conditions.

Similar decrease in layer thickness when increasing the salt concentration in the surrounding solution was also observed for graft-modified porous supports comprising of tentacles with ionic groups [29,49–51]. The grafted tentacles try to avoid strong electrostatic repulsion between adjacent tentacles in low ionic strength buffers by being as far away from each other as possible so they extend. Addition of salt to the surrounding solution screens the repulsive electrostatic interactions, which causes the tentacles to shrink so their layer thickness decreases. Since in the case of grafted tentacles the interaction of the ionized tentacles with the basic surface is negligible, the behavior of the tentacles is influenced mostly by solution conditions what is in agreement with the behavior of the plasmid radius of gyration in the free solution and adsorbed plasmid layer thickness at high salt concentrations. However, adsorbed plasmid layer thickness at low ionic strength solutions is highly dependent on attractive plasmid–surface interactions that cause the decrease of the layer thickness in that range which differs from the behavior of grafted tentacles.

To further examine the behavior of the adsorbed plasmid layer pressure drop measurements during binding capacity measurements at different flow rates were performed and analyzed. While the capacity for 39.4 kbp plasmid was practically flow unaffected (Table 6) that was not the case for inversed permeability increase with mass of loaded plasmid. Surprisingly, as seen from Table 6 inversed permeability (permeability) seemed to increase (decrease) faster when plasmid sample was loaded onto a column at lower flow rate. The final layer thickness at higher linear flow velocities was 20% lower as it was at 120 cm/h. That could be explained by two separate effects which both arise from the specific shape of the plasmid molecule. First explanation is based on the molecule orientation at various flow rates. Tested plasmids are very large hairy-like molecules with the length of more than 1 μm (see Fig. 1) which is in the range of the monolith pore size diameter (1.4 μm). Thus, comparing plasmid dimensions and average pore diameter of the monolithic support, one can speculate that large plasmid cannot penetrate into the pore in any orientation, hence, to pass the monolith without a damage, the molecule has to partly orient along the flow direction so its hydrodynamic diameter would be smaller as the pore diameter [52]. It has been shown that using very low flow velocities, *i.e.*, low share rates, considerable part of DNA molecules is orientated perpendicular to the flow direction [53]. With increasing shear rate (by increasing linear flow velocity) the molecules tend to align more towards the flow direction [53,54]. Considering this, it is theoretically possible that there are molecules that adsorb on the monolith across the pore. That would cause higher pressure drop increase during plasmid loading and slightly higher binding capacity. However, such a binding of the molecules could also cause pore clogging which did not happen in our case. Second explanation issues from the assumption that part of nonadsorbed plasmid tentacles freely moves above the monolithic surface and their position at lower flow rates is more upright regarding the surface, therefore, they extend deeper into the pore and the layer thickness is bigger (for illustration see Fig. 8b).

That the adsorbed plasmid layer is not fixed but rather flexible was also observed by another experiment, where after the adsorption of plasmid at 0.4 M NaCl concentration in binding buffer the monolith was washed by buffer without the salt (pure TE buffer) and pressure drop was measured. No plasmid desorption occurred, but surprisingly, the pressure drop on the column decreased. The layer thickness shrank to 82 nm, which is practically the same as the value obtained directly from capacity measurements in binding buffer without salt (85 nm) whereas the mass of loaded plasmid was approximately 3-times higher. This shows that the layer thickness seems to be a function of the state and not the path (how this state was obtained), what is again similar to the grafted layers on chromatographic monoliths. However, the significant decrease of pressure drop on the monolith with adsorbed plasmid in buffer with lower ionic strength is the opposite to the small increase of pressure drop on grafted monolith comprising tentacles with

Table 7
Data for various sized plasmids obtained from capacity measurements.

Plasmid size, kbp	4.7	21	39.4	62.1	Maximal RSD[a], %
C_{NaCl}[b], M	0.1	0.4	0.4	0.5	/
DBC_{max}[c], mg/mL	9.0	7.1	12.4	8.4[d]	±7
Recovery, %	95	96	84	51	±8
$1/(B_o \cdot m_{pDNA})$[e], $m^{-2}\ \mu g^{-1}$	1.1E+12	1.5E+13	2.2E+13	6.2E+13	±15%
h[f], nm	27	123	172	342	±20%
ρ[g], mg/mL	39	7.0	8.4	2.8	±25%

[a] Relative standard deviation.
[b] NaCl concentration in binding buffer where the dynamic binding capacity for the plasmid was maximal.
[c] Maximal dynamic binding capacity at 50% of breakthrough measured on CIM DEAE monolithic column (CV 12 μL) with 1400 nm average pore diameter and 2.8 mmol/g ligand density at 240 cm/h.
[d] The capacity for 62.1 kbp plasmid was measured at linear flow velocity of 95 cm/h.
[e] Slope coefficients of inversed permeability increase with mass of adsorbed plasmid.
[f] Adsorbed plasmid layer thickness calculated from pressure drop measurements using Eqs. (1), (3) and (4).
[g] Spatial adsorbed plasmid layer density.

anion exchange groups, which means that plasmid layer in buffer with lower ionic strength stabilize itself by shrinking (layer density approximately doubles), while the grafted tentacles try to avoid strong electrostatic repulsion between adjacent tentacles in low ionic strength buffer by extension [29,49–51]. That also shows that plasmid layer with adsorbed salt cations from the buffer seems to be really non-permeable to the mobile phase, since the buffer without salt could not penetrate into the layer itself and cause destabilization but it rather flows above the adsorbed layer that shrank to avoid the low ionic strength shock. Last results again confirm the uniqueness of the adsorbed plasmid system over the grafted systems. Since ionized grafted systems usually includes only repulsive electrostatic interactions (the exception would be mixed mode systems), the adsorbed plasmid system comprises both attractive and repulsive electrostatic interactions the sum of which sometimes leads to unexpected response of the adsorbed layer to the changes of the environmental solution.

Pressure drop data were measured for all four plasmids on the monolithic column with the average pore diameter of 1400 nm and parameters such as inversed permeability increase with mass of adsorbed plasmid, layer thickness and layer density were determined. As it can be seen from Table 7, pressure drop or inversed permeability raised faster with a mass of adsorbed plasmid if the plasmid was larger. So layer thickness also depended on the plasmid size and was bigger for larger plasmids. On the other hand, the adsorbed layer density decreased with increasing plasmid size. To cross check the method for evaluation of layer thickness also the layer thickness of 62.1 kbp plasmid adsorbed on the monolith with 2100 nm average pore diameter at the same salt concentration but higher flow rate was calculated and was determined to be 285 nm which differs from the calculated adsorbed layer thickness on the monolith with smaller pores (being 342 nm – see Table 7). If the layer thickness for certain plasmid depends mostly on stationary phase and solution conditions (*i.e.*, AEX group density and binding buffer composition) and the pore size of monolith is not the limited factor (which can be concluded from similar ratios of specific surface areas and binding capacities on both monoliths, see Table 4), the layer thickness for both monoliths should be the same. Since binding capacities of 62.1 kbp plasmid for monoliths with 1400 nm and 2100 nm average pore diameters were performed at different linear flow velocities (95 and 240 cm/h, respectively), it is possible that the results are not directly comparable (see also Table 6). Therefore, the ratio of layer thicknesses for 39.4 kbp plasmid at 120 and 240 cm/h flow velocities was calculated (1.22) and used to correct the calculated layer thickness for 62.1 kbp plasmid measured at 95 cm/h. The corrected layer thickness for higher flow rates was estimated to 280 nm, which is practically the same as measured layer thickness at monolith with larger pores and linear flow velocity 240 cm/h. Using corrected layer thickness value for 62.1 kbp plasmid and measured values for other plasmids from Table 7 the linear relationship with plasmid size was obtained (Fig. 9). Similar layer thickness and the fact that capacity ratio for 62.1 kbp plasmid for monoliths with 1400 and 2100 nm pore diameter was the same as specific surface area ratio for both monoliths (see Table 4) indicate that layer density is independent on pore size. Calculated layer densities of adsorbed 62.1 kbp plasmid for 1400 and 2100 nm pore size monoliths were 3.4 and 3.5 mg/mL, respectively (layer density for 1400 nm was calculated from corrected layer thickness). Therefore, the accessibility of the surface on both monoliths is the same and the topology seems to be very similar.

Much smaller adsorbed layer density for large plasmids shows that large plasmids cannot form so dense layers on the monolithic surface. That could be the consequence of stronger repulsive forces between adjacent molecules of large plasmids or steric hindrance problem because of highly branched molecule structure.

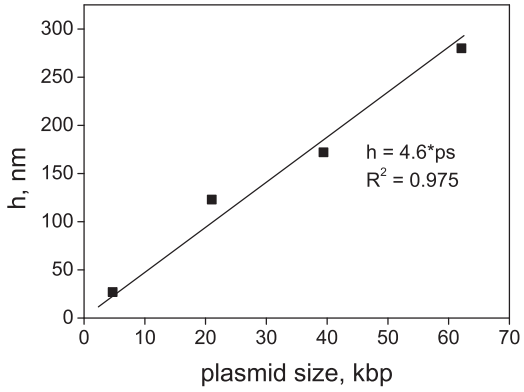

Fig. 9. Correlation of adsorbed plasmid layer thickness and plasmid size.

Both effects would cause sparse molecule distribution on a surface and thus low layer density.

Besides information about the characteristics of adsorbed layer, pressure drop measurements also enable estimation of the pressure drop on a various column scales. Having layer thickness for certain adsorbed plasmid one can calculate change of permeability for a certain pore diameter. The largest CIM monolithic column unit has a volume of 8 L with the pore radius of approximately 1500 nm exhibiting pressure drop of around 1.5 bar at 10 L/min. Taking into account thickness of adsorbed plasmid layer to be 30, 120, 175, 270 nm for plasmids of 5, 20, 40 and 62 kbp in size, the permeability decrease would be 1.3-, 3-, 4.8- and 11-fold, respectively. Therefore, the pressure drop on the monolithic column at 10 L/min would be only 2, 4.5, 7.2 and 16.5 bar, which is acceptable for most of the preparative chromatographic systems. The only exception might be purification of the largest plasmid, where the flow-rate should be decreased at the end of loading.

4. Conclusions

High capacity and recovery of large plasmids purified on CIM monolithic columns suggest that efficient monolith based downstream processes can be developed for plasmids of at least up to 60 kbp. Measuring the pressure drop on a small monolithic column during loading gives information necessary to design large scale process in terms of productivity and equipment requirements as well as gives guidelines for optimization of the monolith structure itself. Furthermore, thickness and density of adsorbed layer derived from these measurements provide insight on adsorption behavior of studied plasmids. Since this methodology can be easily extended to other large molecules like large proteins, viruses and even cells, it can be considered as a universal frame for evaluation of convective based media.

Acknowledgements

Support of this research by the L'Oréal/UNESCO/The Slovenian Science Foundation through "For Women in Science" National Fellowship (N.L.K.), the Ministry of Higher Education, Science and Technology and the Ministry of the Economy of Slovenia through project L2-2283, program P4-0369 and grant No. 3311-03-831830 (N.L.K.) is gratefully acknowledged. We thank Dr. Ita Junkar from Jožef Stefan Institute for monitoring AFM images and Dr. Matija Tomšič from Faculty of Chemistry and Chemical Technology University of Ljubljana for measuring viscosities. The Centre of Excellence for Biosensors, Instrumentation and Process Control is an operation financed by the European Union, European Regional Development Fund and Republic of Slovenia, Ministry of Higher Education, Science and Technology.

References

[1] F. Sousa, D.M.F. Prazeres, J.A. Queiroz, Trends Biotechnol. 26 (2008) 518.
[2] http://www.wiley.co.uk/genmed/clinical/.
[3] P.J. Bergman, M.A. Camps-Palau, J.A. McKnight, N.F. Leibman, D.M. Craft, C. Leung, J. Liao, I. Riviere, M. Sadelain, A.E. Hohenhaus, P. Gregor, A.N. Houghton, M.A. Perales, J.D. Wolchok, Vaccine 24 (2006) 4582.
[4] http://www.emaxhealth.com/117/10535.html.
[5] http://regulatoryaffairs.pharmaceutical-business-review.com/news/fda_approves_anges_spa_on_collategene_trial_for_pad_100112/.
[6] D.L. Doolan, S.L. Hoffman, Int. J. Parasitol. 31 (2001) 753.
[7] D.H. Barouch, A. Craiu, M.J. Kuroda, J.E. Schmitz, X.X. Zheng, S. Santra, J.D. Frost, G.R. Krivulka, M.A. Lifton, C.L. Crabbs, G. Heidecker, H.C. Perry, M.-E. Davies, H. Xie, C.E. Nickerson, T.D. Steenbeke, C.I. Lord, D.C. Montefiori, T.B. Strom, J.W. Shiver, M.G. Lewis, N.L. Letvin, Proc. Natl. Acad. Sci. U. S. A. 97 (2000) 4192.
[8] J.R. Mascola, G.J. Nabel, Curr. Opin. Immunol. 13 (2001) 489.
[9] A.H. Ellebedy, R.J. Webby, Vaccine 27 (2009) D65.
[10] M. Hoare, M.S. Levy, D.G. Bracewell, S.D. Doig, S. Kong, N. Titchener-Hooker, J.M. Ward, P. Dunnill, Biotechnol. Progr. 21 (2005) 1577.
[11] S. Kong, N. Titchener-Hooker, M.S. Levy, J. Membr. Sci. 280 (2006) 824.
[12] J. Urthaler, W. Buchinger, R. Necina, Chem. Eng. Technol. 28 (2005) 1408.
[13] C.S. Lengsfeld, T.J. Anchordoquy, J. Pharm. Sci. 91 (2002) 1581.
[14] P.H. Oliveira, K.J. Prather, D.M.F. Prazeres, G.A. Monteiro, Trends Biotechnol. 27 (2009) 503.
[15] R. Vázquez, J.E. Brito, M. Pérez, R. Silva, A. Seralena, S. Dueñas-Carrera, M.C. Frontela, A.M. Herrera, Biotechnol. Appl. 22 (2005) 251.
[16] K.J. Prather, S. Sagar, J. Murphy, M. Chartrain, Enzyme Microb. Technol. 33 (2003) 865.
[17] M.M. Diogo, J.A. Queiroz, D.M.F. Prazeres, J. Chromatogr. A 1069 (2005) 3.
[18] A. Jungbauer, J. Chromatogr. A 1065 (2005) 3.
[19] N.R. Deshmukh, A.M. Lali, J. Chromatogr. B 818 (2005) 5.
[20] P. Tiainen, P.-E. Gustavsson, A. Ljunglöf, P.-O. Larsson, J. Chromatogr. A 1138 (2007) 84.
[21] M. Benčina, A. Podgornik, A. Štrancar, J. Sep. Sci. 27 (2004) 801.
[22] A. Zöchling, R. Hahn, K. Ahrer, J. Urthaler, A. Jungbauer, J. Sep. Sci. 27 (2004) 819.
[23] N. Lendero Krajnc, F. Smrekar, J. Černe, P. Raspor, M. Modic, D. Krgović, A. Štrancar, A. Podgornik, J. Sep. Sci. 32 (2009) 2682.
[24] F. Smrekar, A. Podgornik, M. Ciringer, S. Kontrec, P. Raspor, A. Štrancar, M. Peterka, Vaccine 28 (2010) 2039.
[25] M.A. Teeters, S.E. Conrardy, B.L. Thomas, T.W. Root, E.N. Lightfoot, J. Chromatogr. A 989 (2003) 165.
[26] H.C. Birnboim, J. Doly, Nucleic Acids Res. 7 (1979) 1513.
[27] M.M. Bradford, Anal. Biochem. 72 (1976) 248.
[28] M. Barut, A. Podgornik, M. Merhar, A. Štrancar, in: F. Švec, T.B. Tennikova, Z. Deyl (Eds.), Monolithic Materials, Elsevier, Amsterdam, 2003, p. 66.
[29] V. Frankovič, A. Podgornik, N. Lendero Krajnc, F. Smrekar, P. Krajnc, A. Štrancar, J. Chromatogr. A 1207 (2008) 84.
[30] D.R. Latulippe, A.L. Zydney, J. Membr. Sci. 329 (2009) 201.
[31] H. Benoit, P. Doty, J. Phys. Chem. 57 (1953) 958.
[32] G.S. Manning, Biophys. J. 91 (2006) 3607.
[33] J. Urthaler, R. Schlegl, A. Podgornik, A. Štrancar, A. Jungbauer, R. Necina, J. Chromatogr. A 1065 (2005) 93.
[34] M.S. Levy, I.J. Collins, S.S. Yim, J.M. Ward, N. Titchener-Hooker, P. Ayazi-Shamlou, P. Dunnill, Bioprocess Eng. 20 (1999) 7.
[35] S. Yamamoto, M. Nakamura, C. Tarmann, A. Jungbauer, J. Chromatogr. A 1144 (2007) 155.
[36] S. Yamamoto, N. Yoshimoto, C. Tarmann, A. Jungbauer, J. Chromatogr. A 1216 (2009) 2616.
[37] K. Benčina, M. Benčina, A. Podgornik, A. Štrancar, J. Chromatogr. A 1160 (2007) 176.
[38] E.I. Trilisky, A.M. Lenhoff, Biotechnol. Bioeng. 104 (2009) 127.
[39] D.M.F. Prazeres, Biotechnol. Bioeng. 99 (2008) 1040.
[40] A. Podgornik, J. Jančar, M. Merhar, S. Kozamernik, D. Glover, K. Čuček, M. Barut, A. Štrancar, J. Biochem. Biophys. Methods 60 (2004) 179.
[41] Y. Yuan, M.R. Oberholzer, A.M. Lenhoff, Colloids Surf. A 165 (2000) 125.
[42] M. Merhar, Dissertation Thesis, University of Ljubljana, Faculty of Chemistry and Chemical Technology, Ljubljana, 2005.
[43] Y.L. Lyubchenko, L.S. Shlyakhtenko, Proc. Natl. Acad. Sci U. S. A. 94 (1997) 496.
[44] M. Hammermann, N. Brun, K.V. Klenin, R. May, K. Tóth, J. Langowski, Biophys. J. 75 (1998) 3057.
[45] E. Arkhangelsky, B. Steubing, E. Ben-Dov, A. Kushmaro, V. Gitis, Desalination 227 (2008) 111.
[46] K. Ager, D.R. Latulippe, A.L. Zydney, J. Membr. Sci. 344 (2009) 123.
[47] C. Tarmann, A. Jungbauer, J. Sep. Sci. 31 (2008) 2605.
[48] H.N. Endres, J.A.C. Johnson, C.A. Ross, J.K. Welp, M.R. Etzel, Biotechnol. Appl. Biochem. 37 (2003) 259.
[49] J. Hautojärvi, K. Kontturi, J.H. Näsman, B.L. Svarfvar, P. Viinikka, M. Vuoristo, Ind. Eng. Chem. Res. 35 (1996) 450.
[50] K. Kontturi, S. Mafé, A. Manzanares, B.L. Svarfvar, P. Viinikka, Macromolecules 29 (1996) 5740.
[51] Y. Tao, G. Carta, J. Chromatogr. A 1211 (2008) 70–79.
[52] T. Hirasaki, T. Sato, T. Tsuboi, H. Nakano, T. Noda, A. Kono, K. Yamaguchi, K. Imada, N. Yamamoto, H. Murakami, S. Manabe, J. Membr. Sci. 106 (1995) 123.
[53] P. LeDuc, C. Haber, G. Bao, D. Wirtz, Nature 399 (1999) 564.
[54] D.R. Latulippe, K. Ager, A.L. Zydney, J. Membr. Sci. 294 (2007) 169.